July 2026
Volume 2
Issue 3

Interdisciplinary Journal of Civil Engineering
Shahid Beheshti University

DOI: 10.48308/ijce.2026.247450.1035

Comparative Numerical Assessment of UHPC and GFRP Strengthening for Masonry-Infilled Reinforced Concrete Frame under Cyclic Loading

Authors:

Mehdi Ebadi-Jamkhaneh[1, *]

Abstract

This study numerically investigates the cyclic in-plane behavior of seven reinforced concrete (RC) frame configurations to evaluate the effects of masonry infill walls, wall openings, and strengthening techniques using ultra-high-performance concrete (UHPC) and glass-fiber-reinforced polymer (GFRP). Nonlinear finite element models were developed in ABAQUS using the concrete damage plasticity (CDP) model and validated against experimental results. The effects of different infill configurations and strengthening systems were assessed in terms of lateral strength, stiffness degradation, energy dissipation, ductility, and equivalent viscous damping. The results indicate that fully infilled frames exhibit an 82.4% increase in maximum positive lateral resistance compared with the bare frame, whereas a 30% opening reduces the contribution of masonry infills. UHPC strengthening provides the greatest improvement in lateral resistance, with the BFW-UHPC model achieving a maximum positive force of 511.82 kN and accumulated energy absorption of 277.7 kN·m. Conversely, GFRP-strengthened configurations demonstrate a more favorable ductility response. The highest equivalent viscous damping ratio, 13.02%, is obtained for the BFWO-GFRP model. These findings highlight the distinct benefits of UHPC and GFRP for seismic strengthening of masonry-infilled RC frames.

Keywords: Masonry Infill Walls, Wall Openings, UHPC Strengthening, GFRP Strengthening, Cyclic Behavior

1. Department of Civil Engineering, School of Engineering, Damghan University, Damghan, Iran

*Corresponding Author: m.ebadi@du.ac.ir

1. Introduction

Reinforced concrete (RC) moment-resisting frames with masonry infill walls represent one of the most widely used structural systems in residential and commercial buildings worldwide. Masonry infills are generally considered non-structural components and are primarily intended to provide architectural separation, thermal insulation, and acoustic protection. However, numerous experimental and numerical investigations have demonstrated that their interaction with the surrounding RC frames can substantially influence the overall structural response, particularly under lateral and seismic loading. Although masonry infill walls are frequently neglected in conventional structural design and analysis, their contribution to lateral stiffness, strength, energy dissipation, and deformation capacity can be significant. The interaction between masonry panels and their surrounding frames may also modify the distribution of internal forces and alter the anticipated failure mechanisms of structural members. Consequently, ignoring the mechanical contribution of masonry infills may lead to inaccurate predictions of the seismic performance of RC buildings (Mehrabi et al. 1996; Dias-Oliveira et al. 2022).

Under lateral loading, masonry infill panels interact with the surrounding beams and columns through contact and friction mechanisms, resulting in the development of diagonal compressive struts. This mechanism generally increases the initial lateral stiffness and load-carrying capacity of the structural system while reducing lateral displacements. Nevertheless, the relatively low tensile strength and limited deformation capacity of conventional masonry materials can result in brittle cracking, sliding along mortar joints, diagonal compression failure, and local crushing near the corners of the infill panels. Furthermore, the interaction between the infill and the surrounding frame may introduce undesirable effects, including short-column behavior, increased shear demand in columns, and unexpected redistribution of seismic forces. These phenomena indicate that the contribution of masonry infills should not be evaluated exclusively in terms of their beneficial effects on lateral strength; their potential influence on structural damage and seismic vulnerability must also be considered (Al-Chaar et al. 2002; Messaoudi et al. 2022; Pokharel et al. 2024).

One of the important parameters governing the seismic behavior of masonry-infilled RC frames is the presence, size, and configuration of openings within the infill panels. Openings are commonly required for architectural and functional purposes, including windows, doors, ventilation systems, and building services. However, openings interrupt the diagonal compression load-transfer mechanism and reduce the masonry panel's effective resisting area. Depending on their dimensions and locations, openings may also produce localized stress concentrations, modify the interaction between the masonry panel and surrounding columns, and promote the development of relatively narrow wall segments. Consequently, the lateral strength, stiffness, energy dissipation capacity, and failure mechanisms of infilled frames can be significantly affected. Arslan et al. (2022) demonstrated that opening size and arrangement

influence the cyclic response of aerated concrete block-infilled RC frames, with larger openings generally reducing load-carrying and energy dissipation capacities. Similarly, Di Trapani et al. (2024) experimentally investigated the influence of different opening configurations on the cyclic response of masonry-infilled RC frames and reported that opening geometry and location substantially modify the resisting mechanisms and damage development. More recently, Milijaš et al. (2023) examined the behavior of fully and partially infilled RC frames under combined in-plane and out-of-plane loading, highlighting the importance of considering openings when evaluating the seismic performance of masonry infills.

Given the limitations associated with conventional masonry infills, various strengthening and retrofitting techniques have been developed to improve their seismic performance without requiring complete removal or replacement of existing wall panels. Among these techniques, externally bonded fiber-reinforced polymer (FRP) composites have attracted considerable attention because of their high tensile strength, low weight, corrosion resistance, and relatively straightforward installation. Glass fiber-reinforced polymer (GFRP), in particular, offers an attractive strengthening alternative because of its favorable mechanical properties and potential for application to existing masonry surfaces. When properly bonded to masonry, GFRP sheets can bridge developing cracks, improve the integrity of the wall panel, and facilitate the redistribution of tensile stresses. These mechanisms may delay crack propagation, reduce the likelihood of premature separation of masonry units, and improve the deformation capacity of strengthened walls. Almusallam and Al-Salloum (2007) demonstrated the effectiveness of GFRP sheets in improving the in-plane seismic response of masonry infill walls within RC frames. More recent investigations by Arslan et al. (2022) demonstrated that glass fiber-reinforced cementitious plaster can improve the cyclic performance of brick infill walls, particularly in terms of lateral resistance, stiffness degradation, and energy dissipation. Furthermore, Kanani Kashani et al. (2023) reported improvements in the load-carrying capacity and deformation performance of masonry walls strengthened using near-surface-mounted GFRP reinforcement under cyclic loading. These findings support the potential of fiber-based composite systems as effective solutions for improving the seismic resistance of masonry components.

Another promising strengthening approach involves the application of ultra-high-performance concrete (UHPC) as an external protective and reinforcing layer. UHPC is characterized by its high compressive strength, improved tensile performance, dense microstructure, and enhanced resistance to crack propagation, particularly when steel fibers are incorporated into its composition (Graybeal 2006). Compared with conventional cement-based mortars, UHPC can provide a more effective load-transfer mechanism and improve the structural integrity of strengthened components. When applied as a thin overlay on masonry surfaces, UHPC may contribute to the development of a composite resisting system in which the original masonry panel and the strengthening layer interact to resist lateral forces. The effectiveness of this

approach, however, depends on several parameters, including overlay thickness, interface bond characteristics, fiber content, anchorage configuration, and the mechanical compatibility between the strengthening material and the masonry substrate. Recent research has increasingly explored UHPC-based solutions for strengthening existing masonry and RC structural components. In particular, the experimental investigation of masonry-infilled RC frames strengthened using precast UHPC diagonal strips demonstrated the potential of this material to enhance lateral resistance under cyclic loading (Sleiman et al. 2024). Such findings suggest that UHPC overlays may offer an effective alternative to conventional strengthening methods, although their performance under different infill configurations requires further investigation.

Despite the growing interest in advanced strengthening materials, several aspects of the seismic behavior of strengthened masonry-infilled RC frames remain insufficiently understood. In particular, the interaction between strengthening materials and masonry panels containing openings introduces additional complexities. Openings may interrupt the continuity of the strengthening layer and create stress concentrations around their boundaries. In addition, the effectiveness of a strengthening technique developed for a solid masonry panel cannot necessarily be assumed to remain unchanged when applied to a panel with openings. Tekeli et al. (2024) investigated the cyclic behavior of masonry-infilled RC frames with openings strengthened using reinforced stucco and demonstrated that although strengthening improved the lateral capacity, initial stiffness, and energy dissipation, the presence and configuration of openings influenced the effectiveness of the strengthening system. Similarly, Kabaş et al. (2023) investigated CFRP strengthening of masonry-infilled RC frames with openings and highlighted the importance of strengthening arrangements in mitigating the adverse effects of openings. These investigations emphasize the need for systematic comparisons of strengthening materials and wall configurations under consistent loading and boundary conditions.

Moreover, the majority of previous investigations have concentrated on individual strengthening techniques or specific masonry configurations, making direct comparisons between different strengthening systems difficult. Studies addressing the simultaneous influence of wall openings and different external strengthening materials on the hysteretic behavior of masonry-infilled RC frames remain particularly valuable. The distinction between improvements in peak lateral strength and improvements in deformation capacity is also important. A strengthening technique may substantially increase lateral resistance and initial stiffness while potentially changing the displacement ductility, post-peak response, and energy dissipation characteristics. Therefore, a comprehensive assessment should consider not only the maximum lateral load but also the evolution of stiffness degradation, hysteretic energy dissipation, residual deformation, and damage progression throughout the loading history.

Against this background, the present study systematically investigates the cyclic behavior of seven RC frame configurations to comparatively evaluate the effects of masonry infill, 30%

wall openings, and two advanced strengthening techniques, namely UHPC and GFRP. The investigated configurations include a bare RC frame, fully and partially infilled frames, and fully and partially infilled frames strengthened with either a 30-mm-thick UHPC overlay or GFRP sheets. The main novelty of this research lies in the direct comparative assessment of UHPC and GFRP strengthening systems for both solid and perforated masonry infills under identical cyclic loading conditions. Unlike studies focusing on individual strengthening techniques or specific infill configurations, this investigation provides a unified framework for examining the interaction between opening-induced weaknesses and strengthening mechanisms. Particular emphasis is placed on quantifying the effectiveness of each strengthening technique in recovering the seismic performance lost due to wall openings. The comparative assessment considers lateral load-carrying capacity, initial stiffness, displacement ductility, stiffness degradation, cumulative energy dissipation, and hysteretic behavior. Furthermore, damage evolution and governing failure mechanisms are examined to identify the advantages and limitations of each strengthening strategy. The results are expected to provide new insights into the development of efficient strengthening solutions for masonry-infilled RC frames, particularly where architectural openings cannot be eliminated.

2. Materials and Methods

2.1. Description of the Numerical Models

Seven numerical models were developed to investigate the effects of masonry infill walls, wall openings, and different strengthening techniques on the in-plane cyclic behavior of RC frames. The models were categorized into four groups based on their infill configurations and strengthening materials. Figure 1 illustrates the numerical models considered in the analyses conducted in this study. Model BF represents a bare RC frame without any masonry infill. Model BFW consists of an RC frame with a fully infilled masonry wall, whereas Model BFWO represents an RC frame with a masonry infill wall containing a centrally located opening. The opening occupies 30% of the total masonry wall area. The fourth and fifth models, designated BFW-UHPC and BFWO-UHPC, correspond to the fully infilled and opening-containing configurations, respectively, strengthened with 40-mm-thick UHPC panels attached to both sides of the masonry wall. Similarly, the sixth and seventh models, designated BFW-GFRP and BFWO-GFRP, represent the corresponding fully infilled and partially opened masonry configurations strengthened with one layer of GFRP on each side of the wall. The configurations and strengthening details of the seven numerical models are summarized in Table 1.

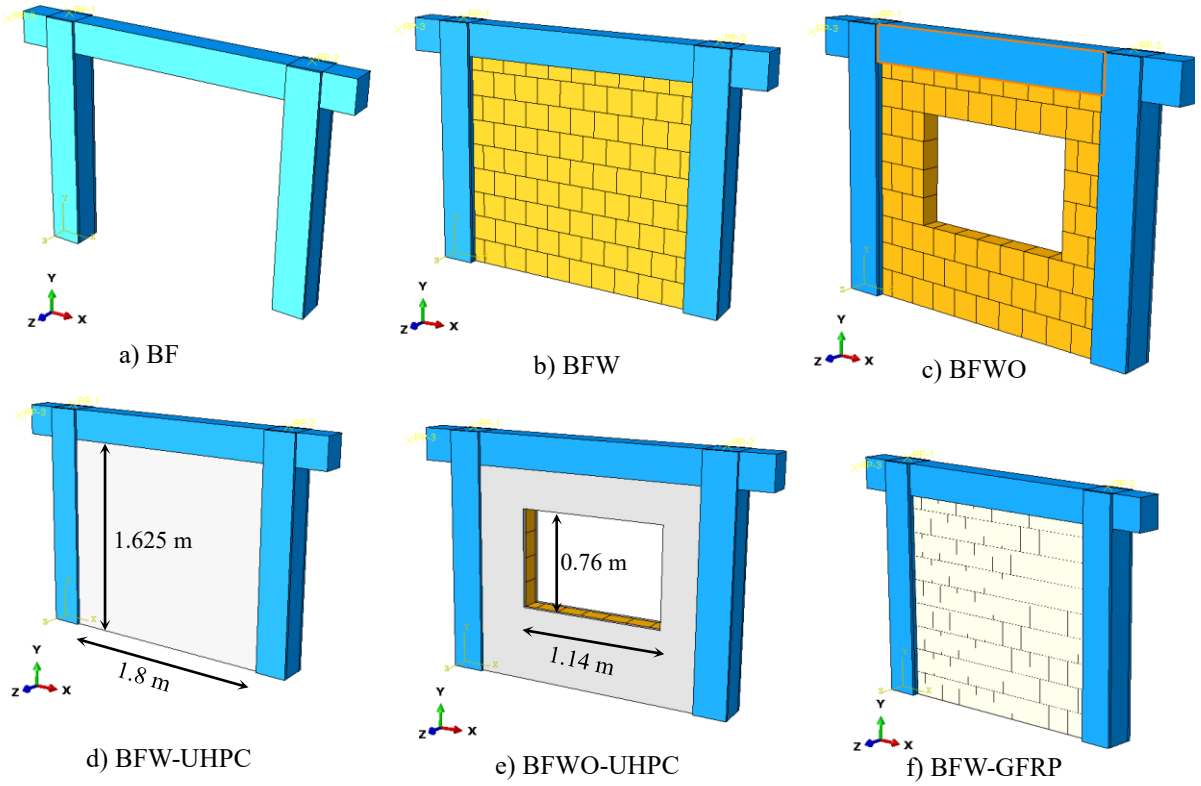


Figure 1. Configuration and geometry of the seven numerical models considered in this study.

Table 1. Description and configuration of the numerical models.

Model	Masonry infill configuration	Strengthening system
BF	No infill	None
BFW	Fully infilled masonry wall	None
BFWO	Masonry wall with a centrally located opening (30% of wall area)	None
BFW-UHPC	Fully infilled masonry wall	40-mm-thick UHPC panels on both sides
BFWO-UHPC	Masonry wall with a centrally located opening (30% of wall area)	40-mm-thick UHPC panels on both sides
BFW-GFRP	Fully infilled masonry wall	One layer of GFRP on each side
BFWO-GFRP	Masonry wall with a centrally located opening (30% of wall area)	One layer of GFRP on each side

2.2. Material Behavioral Model

The CDP model in ABAQUS simulated the nonlinear behavior of concrete structural elements and masonry infills, capturing tensile cracking, compressive crushing, stiffness degradation, and damage evolution. The concrete properties were defined based on the fib Model Code (2013), with a density of 2400 kg/m³, Young's modulus of 22 GPa, Poisson's ratio of 0.15, compressive strength of 30.15 MPa, and tensile strength of 3.0 MPa. The CDP parameters included a dilation angle of 30°, flow potential eccentricity of 0.1, a biaxial-to-uniaxial compressive strength ratio of 1.16, and a tensile-to-compressive meridian parameter of 0.667 (Soalih et al. 2026). The masonry infills were also modelled using CDP, with a density of 1880 kg/m³, Young's modulus of 2901 MPa, Poisson's ratio of 0.20, compressive strength of 9.7 MPa, tensile strength of 0.8 MPa, dilation angle of 34°, and viscosity parameter of 10^{-6} to enhance numerical convergence (Soalih et al. 2026). Tensile and compressive damage characteristics were incorporated for both materials to represent their nonlinear response under seismic loading. The steel components of the building models were simulated using the elastic-plastic material model for ductile metals available in ABAQUS software. The reinforcing steel bars were modelled with a Young's modulus of 200 GPa, a Poisson's ratio of 0.3, and a density of 7850 kg/m³. The steel had a yield strength of 430 MPa and an ultimate tensile strength of 545 MPa (Soalih et al. 2026).

The GFRP sheets were modelled using an orthotropic linear elastic constitutive formulation to account for their direction-dependent mechanical behavior. The elastic properties were adopted from the experimental investigation conducted by Alaskar et al. (2025), which reported an elastic modulus of approximately 60 GPa, an ultimate tensile strength of 1100 MPa, and an ultimate tensile strain of approximately 1.8%. To simulate potential failure of the composite material under cyclic loading, the Hashin damage initiation criterion was considered. This criterion distinguishes between four primary failure mechanisms: fiber tensile failure, fiber compressive failure, matrix tensile failure, and matrix compressive failure. Following damage initiation, an energy-based damage evolution law can be employed to simulate progressive material degradation and stiffness reduction. This formulation provides a framework for capturing the damage response and potential failure of GFRP sheets subjected to cyclic loading.

The mechanical behavior of the UHPC panels was simulated using the CDP model available in ABAQUS. This constitutive model was selected to capture the nonlinear tensile and compressive responses of UHPC, including tensile cracking, compressive crushing, and stiffness degradation under cyclic loading. The compressive and tensile strengths were defined as 115 MPa and 6.2 MPa, respectively, based on the experimental investigation conducted by Hung et al. (2026). The CDP formulation was characterized by a dilation angle of 35° and an eccentricity of 0.1, while the biaxial-to-uniaxial compressive strength ratio and the parameter K_c were set to 1.16 and 0.667, respectively. A viscosity parameter of 0.01 was also adopted to improve numerical stability during the nonlinear analysis.

2.3. Elements

The reinforced concrete (RC) columns, beams, and masonry brick infill walls were modeled using eight-node, three-dimensional solid elements with reduced integration (C3D8R), which capture the complex three-dimensional stress and deformation behavior of these components. The reinforcing steel bars were represented by two-node, three-dimensional truss elements (T3D2) and incorporated into the surrounding concrete using the embedded element technique available in ABAQUS. This approach assumes a perfect bond between the reinforcing steel and the concrete, thereby neglecting any relative slip between the reinforcement and the surrounding concrete matrix. The UHPC panels were also discretized using eight-node, three-dimensional reduced-integration solid elements to accurately represent their three-dimensional stress distribution and nonlinear mechanical response. In contrast, the GFRP sheets were modeled using four-node, quadrilateral, general-purpose shell elements with reduced integration (S4R). These shell elements are particularly suitable for representing the relatively thin GFRP sheets, allowing their in-plane stiffness, bending behavior, and stress distribution to be captured efficiently without requiring a fully three-dimensional solid mesh.

2.4. Contact and Boundary Conditions

The simplified micro-modelling approach proposed by Lourenço (1996) and Abdulla et al. (2017) was adopted to simulate the interaction between masonry units and mortar joints. In this approach, the brick units are represented by continuum elements with dimensions expanded to account for the mortar thickness, while the unit-to-unit interactions are modelled using discontinuous interface elements. This formulation enables the simulation of the mechanical interaction and potential relative displacement between adjacent masonry units without explicitly modelling the mortar joints. The masonry infill–RC frame interface was modelled using surface-to-surface cohesive contact to capture progressive damage and debonding. The normal and shear stiffnesses were 152 and 70 N/mm³, respectively. Damage initiation followed the quadratic nominal stress criterion, with normal and shear strengths of 0.73 and 1.02 MPa. Damage evolution was governed by the Benzeggagh–Kenane (BK) mixed-mode criterion, with Mode I and Mode II fracture energies of 0.012 and 0.05 N/mm, respectively, and a BK exponent of 0.75 (Soalih, Cebir et al. 2026). The reinforcing bars in the RC frame were embedded within the surrounding concrete elements using the Embedded Region constraint in ABAQUS. This technique ensures compatibility between the displacements of the reinforcement and the host concrete, assuming a perfect bond between the two materials. Consequently, relative slip between the reinforcing bars and the surrounding concrete was neglected.

Based on the experimental investigation conducted by Hung et al. (2026) 40-mm-thick UHPC panels were applied to masonry walls, and no noticeable debonding or relative sliding was observed at the interface between the UHPC panels and the masonry substrate. This

experimental observation indicates that a sufficiently strong bond can develop between the two materials, ensuring compatible deformation under the applied loading conditions. Accordingly, in the present numerical model, the interaction between the UHPC panels and the masonry walls was defined using the TIE constraint available in ABAQUS. This constraint enforces displacement compatibility between the two contacting surfaces, preventing relative translational movement and separation at the interface. Therefore, the UHPC panels and masonry walls were assumed to act compositely throughout the loading process, consistent with the experimental observations reported by Hung et al. (2026).

The boundary conditions and loading protocol were defined to reproduce the experimental setup. The bottom ends of the RC columns and masonry walls were fully fixed to prevent any translational and rotational movements. At the upper ends of the beams and columns, translational displacement perpendicular to the plane of loading was restrained to ensure out-of-plane stability while allowing in-plane deformation of the specimens. A cyclic lateral displacement was applied at the top of the beam, in the plane of the masonry wall, to simulate reversed cyclic loading conditions. The loading history followed the displacement-controlled cyclic loading protocol recommended by FEMA 461 (2007), which involves a series of gradually increasing displacement amplitudes to evaluate the structural response under repeated loading cycles (Figure 2). This loading configuration was adopted to investigate the in-plane seismic performance, stiffness degradation, strength deterioration, and hysteretic behavior of the RC frame–masonry infill systems.

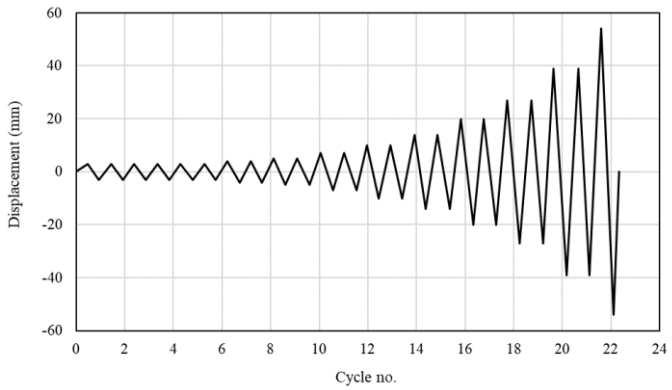
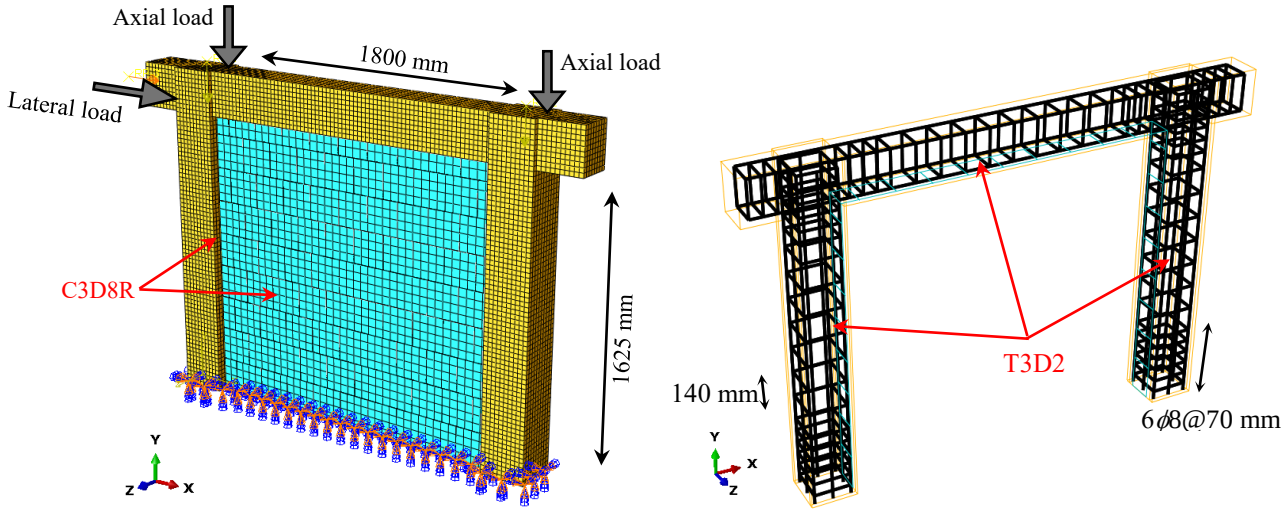


Figure 2. Loading protocol (FEMA 2007).

2.5. Validation of the Numerical Model

The accuracy of the numerical model was validated against the experimental results reported in (Soalih et al. 2026), which investigated the cyclic behavior of RC frames with and without brick masonry infills under displacement-controlled lateral loading. The bare frame geometry and reinforcement details were reproduced, including a 200 × 250 mm beam reinforced with two 12-mm-diameter bars at both the top and bottom, and 250 × 250 mm columns reinforced with eight 12-mm-diameter bars. Transverse reinforcement consisted of 8-mm-diameter bars

spaced at 70 mm in critical regions and 140 mm elsewhere. The clear span and storey height were 1800 and 1625 mm, respectively. The masonry infill was 135 mm thick and constructed using 135 × 190 × 190 mm horizontally perforated clay bricks with 10 mm mortar joints. The concrete compressive strength was 30.15 MPa, and the reinforcing steel yield strength was 430 MPa. A constant axial load of 188.438 kN was applied to each column, equivalent to approximately 10% of its axial load-carrying capacity. The validation model is illustrated in Figure 3.



a) Elements and boundary conditions. **b) Reinforcement details.**

Figure 3. Geometric configuration, dimensions, finite element mesh, and element types adopted in the numerical model.

Validation involved comparing the predicted lateral resistance and initial stiffness with the experimental results for the BF and BRK specimens (Table 2 and Figure 4). For BRK, the errors in maximum positive and negative lateral forces were 9.41% and 1.42%, respectively, while the predicted initial stiffness of 88.35 kN/mm differed from the experimental value of 81.05 kN/mm by 9.01%. For BF, the corresponding errors in maximum positive force, maximum negative force, and initial stiffness were 8.24%, 7.54%, and 7.16%, respectively. These results demonstrate reasonable agreement between the numerical predictions and experimental measurements, supporting the model's suitability for subsequent analyses.

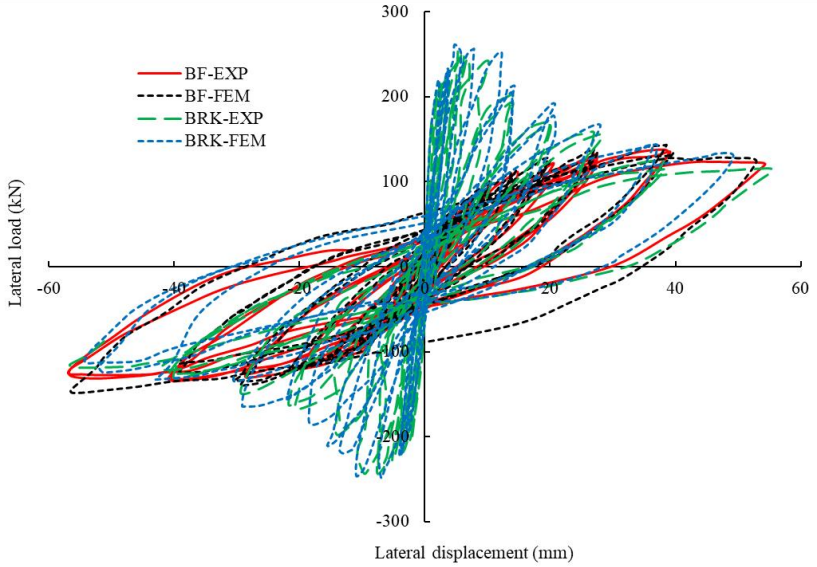
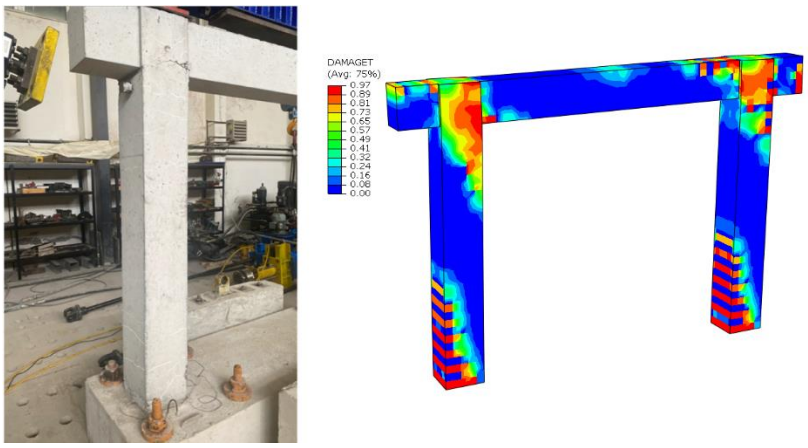


Figure 4. Comparison of the experimentally measured and numerically predicted lateral force–lateral displacement hysteresis responses of the RC frame.

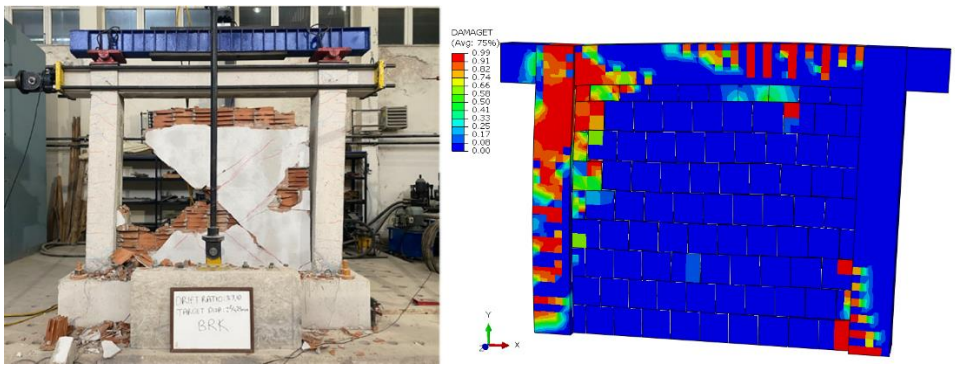
Table 2. Comparison of peak lateral forces and initial stiffness.

Parameter	BF-EXP	BF-FEM	Error (%)	BRK-EXP	BRK-FEM	Error (%)
Maximum positive lateral force, F_{max}^{+} (kN)	132.42	143.33	8.24	238.90	261.38	9.41
Maximum negative lateral force, F_{max}^{-} (kN)	−138.00	−148.40	7.54	−243.45	−246.90	1.42
Initial stiffness, K_0 (kN/mm)	16.90	18.11	7.16	81.05	88.35	9.01

As shown in Figure 5, the numerical model reproduces the main features of the experimentally observed damage in the masonry-infilled RC frame under cyclic loading. In both cases, damage is concentrated near the infill boundaries and masonry-frame interfaces, where stress concentrations and relative slip promote tensile cracking and material degradation. The tensile damage variable (DAMAGET) reaches approximately 0.8–0.99 in severely damaged regions, while much of the central panel exhibits lower values, generally below 0.08-0.23. This distribution agrees qualitatively with the observed cracking, brick detachment, and partial masonry disintegration. Minor discrepancies in damage continuity and extent are expected because the numerical model represents continuum-based tensile degradation. In contrast, experimental failure also involves discrete cracking, mortar-joint separation, and local brick crushing.



a) BF model



b) BRK model

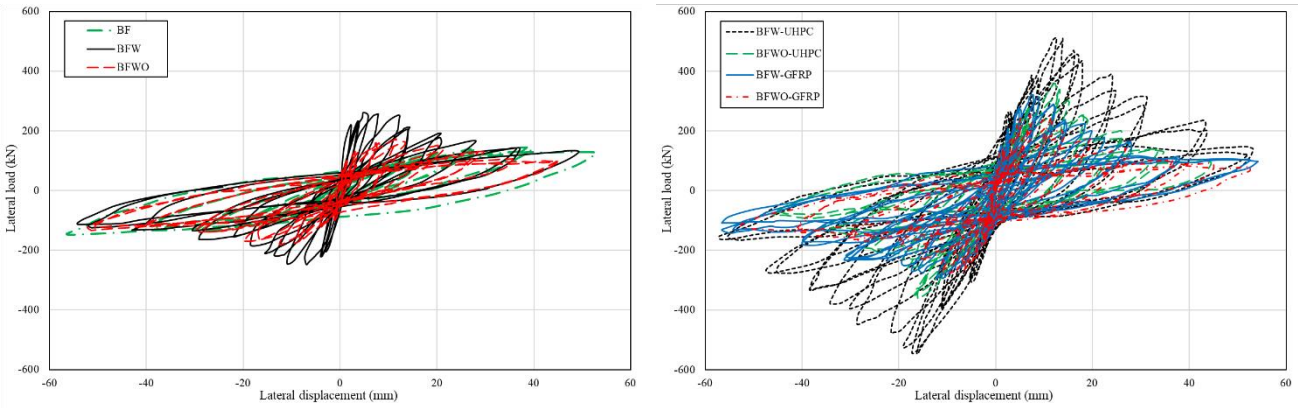
Figure 5. Comparison of the failure patterns and damage mechanisms observed in the experimental specimen and the numerical model.

3. Results and Discussion

3.1. Force-Displacement Relationships

Figure 6 illustrates the force–displacement hysteresis curves of the seven numerical models, highlighting the effects of masonry infill walls, wall openings, and strengthening techniques on their cyclic lateral response. As summarized in Table 3, the fully infilled RC frame (BFW) showed a substantial improvement in lateral load-carrying capacity over the bare frame (BF), reaching a maximum positive force of 261.38 kN, an increase of approximately 82.4%. However, introducing a 30% opening into the masonry infill (BFWO) reduced the maximum positive force to 172.71 kN, demonstrating the detrimental effect of openings on the lateral resistance provided by masonry infills. The most significant enhancement in lateral strength was achieved by the BFW-UHPC model, which attained the highest positive and negative force capacities of 511.82 and −548.13 kN, respectively. The BFWO-UHPC model also exhibited considerable resistance, with corresponding peak forces of 358.64 and −363.89 kN. Regarding

initial stiffness, BFWO-UHPC recorded the highest estimated value of 214.61 kN/mm, followed by BFW (168.38 kN/mm) and BFW-UHPC (138.08 kN/mm). The GFRP-strengthened configurations also improved the lateral resistance relative to the bare frame, although their peak strengths remained lower than those of the corresponding UHPC-strengthened models.



a) Unreinforced models **b) Reinforced models**

Figure 6. Hysteresis curves of the numerical models.

Table 3. Summary of force-displacement response parameters.

Model	P^{+}_{max} (kN)	Δ^{+}_{max}(mm)	P^{-}_{max}(kN)	Δ^{-}_{max} (mm)	$K_{initial}$ (kN/mm)	W_{abs} (kN.m)	μ	ε_{eq}
BF	143.33	38.34	-148.4	-54.58	18.11	80.5	N/A	8.82
BFW	261.38	4.78	-246.9	-6.98	168.38	85.5	2.54	11.41
BFWO	172.71	11.58	-180.53	-12.46	103.15	79.1	2.7	11.84
BFW-UHPC	511.82	12.57	-548.13	-16.07	138.08	277.7	1.84	11.71
BFWO-UHPC	358.64	12.25	-363.89	-16.04	214.61	120.5	1.63	12.74
BFW-GFRP	320.79	7.73	-293.49	-12.24	100.2	168.4	2.46	11.12
BFWO-GFRP	254.04	11.39	-279.73	-10.56	101.52	116.3	2.14	13.02

P^{+}_{max}: Maximum Positive Force; Δ^{+}_{max}: Displacement at Maximum Positive Force; P^{-}_{max}: Maximum Negative Force; Δ^{-}_{max}: Displacement at Maximum Negative Force; $K_{initial}$: Initial Secant Stiffness; W_{abs}: Accumulated Absolute Work; μ: Ductility; ε_{eq}: Equivalent Viscous Damping.

Figure 7 presents the envelope curves extracted from the hysteresis responses of the seven numerical models, providing a comparative assessment of their lateral load-carrying capacity

and deformation characteristics. These curves highlight the influence of masonry infill configuration and strengthening techniques on the overall strength and displacement capacity of the RC frames.

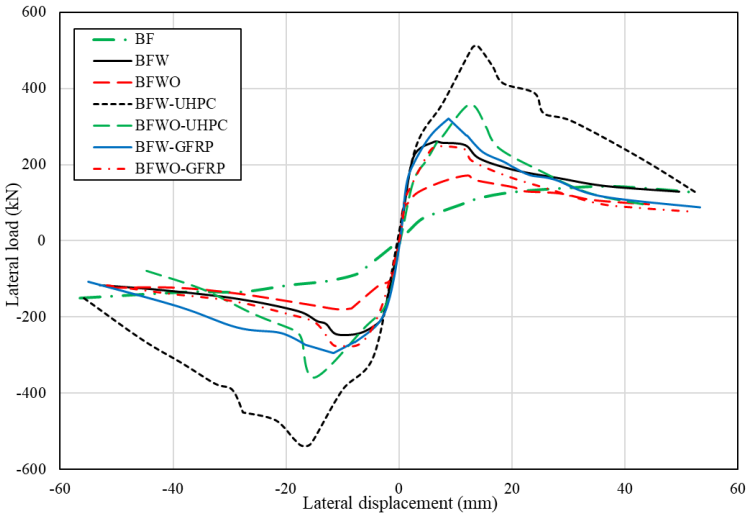


Figure 7. Envelope curves of the force-displacement hysteresis responses for the seven numerical models.

3.2. Cyclic Stiffness Degradation Analysis

Figure 8 illustrates the variation in effective cyclic stiffness over successive loading cycles for the seven numerical models, providing insight into their stiffness degradation characteristics under repeated lateral loading. As shown in the figure, all models exhibit a progressive reduction in stiffness as the number of loading cycles increases. This behavior is primarily attributed to the accumulation of damage within the structural components, including concrete cracking, compressive damage, degradation of the concrete–masonry interaction, and deterioration of the load-transfer mechanisms. The BF exhibits a relatively low initial effective stiffness of 13.01 kN/mm, which decreases to 2.45 kN/mm by the fifteenth cycle, corresponding to an approximately 81.2% reduction. In comparison, the fully infilled frame (BFW) starts at 78.70 kN/mm and reaches 2.36 kN/mm by the fourteenth cycle. The corresponding frame with a 30% masonry opening (BFWO) shows a decrease from 67.12 to 2.35 kN/mm over the same number of cycles. The higher initial stiffness of the infilled configurations compared with the bare frame highlights the contribution of masonry infills to lateral resistance. However, the more pronounced stiffness reduction in these models can be associated with progressive cracking and crushing of the masonry panels, degradation of the frame–infill interface, and the resulting loss of composite action. The presence of the opening further interrupts the continuity of the infill panel and reduces its effectiveness in transferring lateral forces.

The strengthening systems modify both the initial stiffness and its evolution during cyclic loading. The BFW-UHPC model exhibits an initial effective stiffness of 69.06 kN/mm, which

decreases to 2.49 kN/mm by the nineteenth cycle, whereas the corresponding BFWO-UHPC model decreases from 73.48 to 1.91 kN/mm by the sixteenth cycle. For the GFRP-strengthened configurations, the initial stiffness values are 73.91 and 74.26 kN/mm for BFW-GFRP and BFWO-GFRP, respectively, declining to 2.07 kN/mm by the twentieth cycle and 1.93 kN/mm by the seventeenth cycle. The comparatively sustained stiffness of the UHPC- and GFRP-strengthened models over a larger number of cycles indicates that these strengthening materials help preserve the lateral load-transfer capacity and delay the development of severe damage. UHPC panels can improve resistance through their high compressive strength, stiffness, and ability to limit local crushing, while GFRP layers contribute through tensile resistance, crack bridging, and confinement effects. Nevertheless, neither strengthening technique can completely prevent stiffness degradation because repeated reversals progressively damage the surrounding concrete, masonry, and their interfaces. The results also suggest that the effectiveness of a strengthening system should be evaluated not only in terms of its initial stiffness but also by its ability to retain stiffness throughout repeated loading cycles.

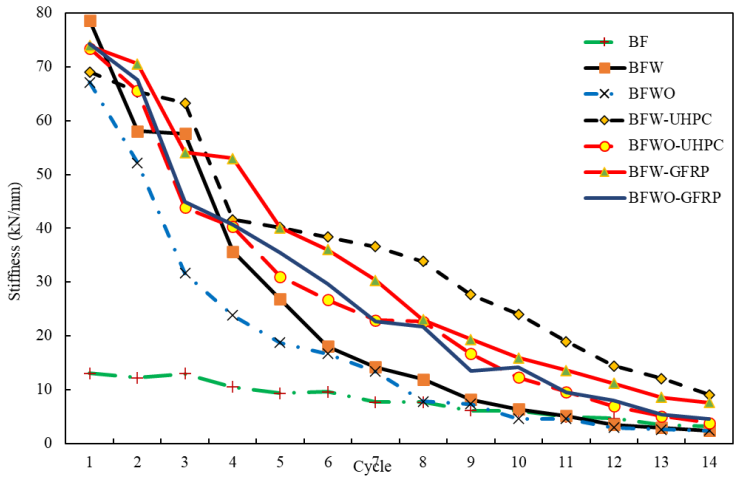


Figure 8. Variation in effective cyclic stiffness with loading cycles for the seven numerical models.

3.3. Cyclic Energy Dissipation Analysis

Figure 9 illustrates the energy dissipated per loading cycle for the seven numerical models. Overall, energy dissipation increases with successive loading cycles, reflecting the progressive development of cracking, plastic deformation, and damage under cyclic loading. The BFW-UHPC model exhibits the highest energy dissipation, reaching approximately 14,860 J in its eighteenth cycle, indicating the substantial contribution of UHPC strengthening to energy absorption. The BFW-GFRP model also demonstrates considerable energy dissipation, reaching approximately 10,851 J in its twentieth cycle. Among the unstrengthened configurations, the BFW model dissipates more energy than the BFWO and BF models, highlighting the beneficial contribution of full masonry infill. The presence of a 30% opening reduces the energy dissipation capacity by interrupting the continuity of the infill panel and

weakening its interaction with the surrounding frame. The improved performance of strengthened models can be attributed to enhanced resistance, crack control, and more effective energy absorption mechanisms.

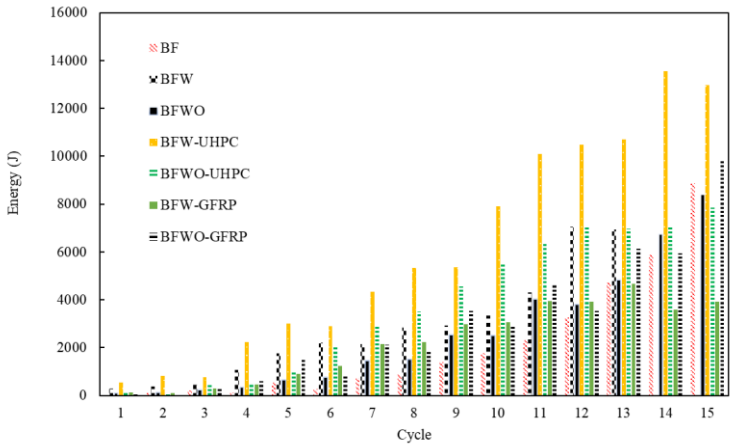


Figure 9. Energy dissipated per loading cycle for the seven numerical models.

3.4. Ductility and Equivalent Viscous Damping Analysis

The ductility ratios (μ) presented in Table 3 reveal considerable differences in the deformation capacity of the investigated models. The BFW model exhibits a ductility ratio of 2.54, while the introduction of a 30% opening increases this value to 2.70, suggesting that the reduced infill continuity allows greater deformation before reaching the defined ultimate limit. Strengthening with UHPC results in lower ductility ratios of 1.84 and 1.63 for the BFW-UHPC and BFWO-UHPC models, respectively. This reduction can be attributed to the increased strength and stiffness provided by UHPC, which may limit the deformation capacity of the strengthened systems. A similar trend is observed for the GFRP-strengthened models, although their ductility ratios are relatively higher, reaching 2.46 for BFW-GFRP and 2.14 for BFWO-GFRP. These findings suggest that GFRP strengthening provides a more favorable balance between strength enhancement and deformation capacity compared with UHPC strengthening.

The equivalent viscous damping ratio was evaluated to quantify the energy dissipation capacity of the seven numerical models under cyclic loading. This parameter represents the energy dissipated through hysteretic behavior relative to the maximum elastic strain energy stored in the structural system. The equivalent viscous damping ratio was calculated using the following expression:

$$\varepsilon_{eq} = \frac{E_D}{4\pi E_S} \tag{1}$$

where E_D denotes the energy dissipated during one complete hysteresis cycle, and E_S represents the maximum elastic strain energy. The latter was estimated as one-half of the product of the maximum force and its corresponding displacement. Accordingly, the equivalent viscous damping ratio was determined for each model at comparable displacement amplitudes to ensure a consistent basis for comparison.

The equivalent viscous damping ratios presented in Table 3 range from 8.82% to 13.02%, indicating differences in the hysteretic energy dissipation capacity of the investigated models. The BF exhibits the lowest damping ratio (8.82%), reflecting its limited energy dissipation capacity in the absence of masonry infill. The introduction of masonry infill increases the damping ratio to 11.41% and 11.84% for the BFW and BFWO models, respectively, owing to the additional energy dissipated through cracking, friction, and interaction between the infill panels and the surrounding RC frame. Strengthening with UHPC further improves the damping performance of the frames, particularly in the presence of an opening, where BFWO-UHPC achieves a damping ratio of 12.74%. Similarly, the BFWO-GFRP model exhibits the highest damping ratio (13.02%), suggesting that GFRP strengthening can enhance hysteretic energy dissipation by improving crack control and maintaining effective load transfer within the infilled frame. In contrast, the BFW-GFRP model shows a relatively lower value of 11.12%.

4. Conclusion

This study numerically investigated the cyclic in-plane behaviour of seven RC frame configurations to evaluate the effects of masonry infill walls, wall openings, and strengthening techniques using UHPC and GFRP. Based on the numerical results, the following conclusions can be drawn:

1. The presence of masonry infill walls considerably enhanced the lateral load-carrying capacity of RC frames. Compared with the BF, the fully infilled configuration (BFW) exhibited an 82.4% increase in maximum positive lateral resistance. However, introducing a 30% opening reduced this resistance by approximately 33.9%, highlighting the adverse effect of openings on infill contribution.
2. UHPC strengthening provided the greatest improvement in lateral strength and energy absorption. The BFW-UHPC model achieved maximum positive and negative lateral resistances of 511.82 and −548.13 kN, respectively. Its accumulated absolute energy absorption reached 277.7 kN·m, substantially exceeding that of the other configurations. Nevertheless, the presence of an opening reduced the effectiveness of UHPC strengthening.
3. GFRP strengthening also improved the lateral resistance and energy absorption of the infilled frames. The maximum positive resistance increased to 320.79 kN for BFW-GFRP and 254.04 kN for BFWO-GFRP. Although these improvements were less pronounced than those obtained using UHPC, GFRP-strengthened

configurations generally exhibited higher ductility ratios, indicating a more favourable balance between strength and deformation capacity.

4. All models experienced progressive stiffness degradation under repeated cyclic loading due to the accumulation of cracking, crushing, and damage at the masonry–frame interfaces. However, UHPC and GFRP strengthening helped maintain lateral stiffness over a greater number of loading cycles, delaying the development of severe damage.

5. The ductility and equivalent viscous damping results revealed different advantages for the two strengthening systems. UHPC strengthening increased lateral strength but reduced the ductility ratios to 1.84 and 1.63 for the fully infilled and partially opened configurations, respectively. In contrast, the corresponding GFRP-strengthened models exhibited ductility ratios of 2.46 and 2.14. Furthermore, the highest equivalent viscous damping ratio (13.02%) was obtained for BFWO-GFRP, followed by BFWO-UHPC (12.74%), demonstrating the effectiveness of these strengthening systems in improving hysteretic energy dissipation.

6. This study was limited to numerical simulations of in-plane cyclic behaviour and a specific set of material properties and strengthening configurations. Future research should consider experimental validation of the proposed strengthening systems, investigate different opening sizes and locations, and examine the effects of out-of-plane loading, varying axial loads, and realistic seismic ground motions to provide a more comprehensive assessment of their performance.

Conflict of Interest

The authors declare that there is no conflict of interest regarding the publication of this paper.

5. References

Abdulla, K. F., Cunningham, L. S., & Gillie, M. (2017). Simulating masonry wall behaviour using a simplified micro-model approach. *Engineering Structures*, *151*, 349–365. https://doi.org/https://doi.org/10.1016/j.engstruct.2017.08.021

Al-Chaar, G., Issa, M., & Sweeney, S. (2002). Behavior of Masonry-Infilled Nonductile Reinforced Concrete Frames. *Journal of Structural Engineering*, *128*(8), 1055–1063. https://doi.org/doi:10.1061/(ASCE)0733-9445(2002)128:8(1055)

Alaskar, A., Ghalla, M., Bazuhair, R. W., Elsamak, G., Emara, M., & Altobgy, M. A. (2025). Seismic rehabilitation of brick masonry walls with central openings using hybrid GFRP configurations. *Journal of Building Engineering*, *111*, 113464. https://doi.org/https://doi.org/10.1016/j.jobe.2025.113464

Almusallam, T. H., & Al-Salloum, Y. A. (2007). Behavior of FRP Strengthened Infill Walls under In-Plane Seismic Loading. *Journal of Composites for Construction*, *11*(3), 308–318. https://doi.org/doi:10.1061/(ASCE)1090-0268(2007)11:3(308)

Arslan, M. E., Aykanat, B., Ayyıldız, M. A., Subaşı, S., & Maraşlı, M. (2022). Effects of basalt and glass fiber composites usage for strengthening on the cyclic behavior of brick infill walls. *Journal of Building Engineering*, *52*, 104405. https://doi.org/https://doi.org/10.1016/j.jobe.2022.104405

beton, f.-f. i. d. (2013). *fib model code for concrete structures 2010*. John Wiley & Sons.

Di Trapani, F., Khan, N. A., Zhou, L., Demartino, C., & Monti, G. (2024). Cyclic response of infilled RC frames with window and door openings: Experimental results and damage interpretation. *Earthquake Engineering & Structural Dynamics*, *53*(1), 43–67. https://doi.org/https://doi.org/10.1002/eqe.4005

Dias-Oliveira, J., Rodrigues, H., Asteris, P. G., & Varum, H. (2022). On the Seismic Behavior of Masonry Infilled Frame Structures. *Buildings*, *12*(8), 1146.

FEMA, A. (2007). 461/Interim Testing Protocols for Determining the Seismic Performance Characteristics of Structural and Nonstructural Components. *Applied Technology Council, Redwood City, CA*, *113*.

Graybeal, B. A. (2006). Material Property Characterization of Ultra-High Performance Concrete [Tech Report].

Hung, C.-C., Wang, Y.-Q., & Yen, C.-H. (2026). Retrofitting of masonry-infilled RC frames using UHPC shotcrete: Full-scale experiments and strength modeling. *Construction and Building Materials*, *537*, 146982. https://doi.org/https://doi.org/10.1016/j.conbuildmat.2026.146982

kashani, H. K., Shakiba, M., Bazli, M., Hosseini, S. M., Mortazavi, S. M. R., & Arashpour, M. (2023). The structural response of masonry walls strengthened using prestressed near surface mounted GFRP bars under cyclic loading. *Materials and Structures*, *56*(6), 112. https://doi.org/10.1617/s11527-023-02201-0

Lourenço, P. J. B. B. (1997). Computational strategies for masonry structures.

Mehrabi, A. B., Shing, P. B., Schuller, M. P., & Noland, J. L. (1996). Experimental Evaluation of Masonry-Infilled RC Frames. *Journal of Structural Engineering*, *122*(3), 228–237. https://doi.org/doi:10.1061/(ASCE)0733-9445(1996)122:3(228)

Messaoudi, A., Chebili, R., Mohamed, H., & Rodrigues, H. (2022). Influence of Masonry Infill Wall Position and Openings in the Seismic Response of Reinforced Concrete Frames. *Applied Sciences*, *12*(19), 9477.

Milijaš, A., Marinković, M., Butenweg, C., & Klinkel, S. (2023). Experimental results of reinforced concrete frames with masonry infills with and without openings under combined quasi-static in-plane and out-of-plane seismic loading. *Bulletin of Earthquake Engineering*, *21*(7), 3537–3579. https://doi.org/10.1007/s10518-023-01664-4

Pokharel, S., Biswal, D. R., Sahoo, K. K., & Dhir, P. K. (2024). Seismic Performance of Masonry-Infilled RC Frames and Its Implications in Design Approach: A Review. *Practice Periodical on Structural Design and Construction*, *29*(2), 03124001. https://doi.org/doi:10.1061/PPSCFX.SCENG-1337

Sleiman, E., Ferrier, E., Michel, L., & Saidi, M. (2024). Seismic behavior of masonry-infilled reinforced concrete frames strengthened using ultra-high performance concrete diagonal strips. *Structures*, *59*, 105790. https://doi.org/https://doi.org/10.1016/j.istruc.2023.105790

Soalih, H. A., Cebir, F., Hüsem, M., Livaoğlu, R., & Demir, S. (2026). Seismic evaluation of RC frames infilled with prefabricated lightweight steel panels and brick masonry. *Engineering Structures*, *366*, 123389. https://doi.org/https://doi.org/10.1016/j.engstruct.2026.123389

Tekeli, H., Yüksel, C., Anıl, Ö., & Mutlu, E. O. (2024). Experimental and numerical investigation of hysteretic earthquake behavior of masonry infilled RC frames with opening strengthened by adding rebar-reinforced stucco. *Bulletin of Earthquake Engineering*, *22*(6), 3169–3207. https://doi.org/10.1007/s10518-024-01905-0

Tekeli Kabaş, H., Ebrahim Kusain, F., & Anıl, Ö. (2023). Experimental behavior of masonry infilled RC frames with openings strengthened by using CFRP strip. *Composite Structures*, *312*, 116873. https://doi.org/https://doi.org/10.1016/j.compstruct.2023.116873